



Article

E-BiT: Extended Bio-Inspired Texture Descriptor for 2D Texture Analysis and Characterization

Steve Tsham Mpinda Ataky  and Alessandro Lameiras Koerich * 

École de Technologie Supérieure, Université du Québec, 1100, rue Notre-Dame Ouest,
Montreal, QC H3C 1K3, Canada; steve.ataky@nca.ufma.br

* Correspondence: alessandro.koerich@etsmtl.ca

Abstract: This paper presents an extended bio-inspired texture (E-BiT) descriptor for image texture characterization. The E-BiT descriptor combines global ecological concepts of species diversity, evenness, richness, and taxonomic indexes to effectively capture texture patterns at local and global levels while maintaining invariance to scale, translation, and permutation. First, we pre-processed the images by normalizing and applying geometric transformations to assess the invariance properties of the proposed descriptor. Next, we assessed the performance of the proposed E-BiT descriptor on four datasets, including histopathological images and natural texture images. Finally, we compared it with the original BiT descriptor and other texture descriptors, such as Haralick, GLCM, and LBP. The E-BiT descriptor achieved state-of-the-art texture classification performance, with accuracy improvements ranging from 0.12% to 20% over other descriptors. In addition, the E-BiT descriptor demonstrated its generic nature by performing well in both natural and histopathologic images. Future work could examine the E-BiT descriptor's behavior at different spatial scales and resolutions to optimize texture property extraction and improve performance.

Keywords: pattern recognition; texture characterization; ecological diversity measures; bio-inspired texture descriptor



Citation: Ataky, S.T.M.; Lameiras Koerich, A. E-BiT: Extended Bio-Inspired Texture Descriptor for 2D Texture Analysis and Characterization. *Electronics* **2023**, *12*, 2086. <https://doi.org/10.3390/electronics12092086>

Academic Editor: Byung-Gyu Kim

Received: 10 March 2023

Revised: 19 April 2023

Accepted: 30 April 2023

Published: 3 May 2023



Copyright: © 2023 by the authors. Licensee MDPI, Basel, Switzerland. This article is an open access article distributed under the terms and conditions of the Creative Commons Attribution (CC BY) license (<https://creativecommons.org/licenses/by/4.0/>).

1. Introduction

Texture analysis seeks to establish the surrounding relationship of texture components and their location with respect to the others (connectivity), the number of components per spatial unit (density), and their commonness (homogeneity) [1]. Models developed in the literature to characterize textures can be divided into statistical and geometric methods [2]. The former aims to compute numerical measures by analyzing how and to what extent some textural properties are distributed. The latter explores distinct types of periodicity within an image and describes the texture therein with the relative spectral energy at distinct periodicities.

Texture characterization is not trivial, as this process presents considerable challenges, one of which is related to the capture conditions of images. Accordingly, lighting geometry or intensity changes can significantly impact a textural image's appearance. Moreover, in both the microtexture and macrotexture, different texture types may constrain the characterization process and the definition of methods robust enough to represent texture information within an image, especially when both are present. Indeed, each texture mentioned above contains intrinsic properties that may require a specific statistical method to be represented to the maximum extent. This process involves image processing techniques in computer vision to characterize an image's texture parameters. These techniques allow the extraction of descriptors from an image or a region related to characteristics that refer to intrinsic properties such as roughness, regularity, smoothness, etc. Thus, choosing which texture analysis method to employ for extracting features becomes challenging for the success of the classification phase. In addition, the metric used in the comparison of feature vectors is also crucial.

A variety of classical and novel methods for texture information extraction from images have been developed and employed successfully, such as gray-level co-occurrence matrix (GLCM) [3], Haralick descriptors [4], local binary patterns (LBPs) [5], wavelet transform [6], Markov random fields [7], histogram of oriented gradients, and fractal models [8]. Other interesting works exploring texture analysis can be found in [9–11], and a review of most of these approaches can be found in [12,13].

Convolutional neural networks (CNNs) have recently drawn the interest of researchers due to their effectiveness in several tasks, such as the detection, segmentation, and classification of objects. CNNs learn abstract features and concepts directly from images [14], with increasing complexity as the images go through many convolutional layers (CLs). The first CLs learn features such as edges and simple textures. The intermediate CLs learn more complex textures and patterns, and the last CLs learn objects or their parts [14]. Andreczyk and Whelan [15] created a straightforward texture CNN architecture (T-CNN) for analyzing texture images that merges an energy measure at the final convolution layer and dumps the general shape information analyzed by conventional CNNs. Despite the encouraging results, the trade-off between complexity and accuracy is not advantageous. Other texture CNN architectures have also reached a reasonable texture classification performance [16–19]. Another drawback of CNNs is their inability to be explained and interpreted.

In most cases, current approaches for texture analysis focus on specific information within images. Accordingly, such approaches usually choose a limited set of texture features from contextual information in the form of a region of interest. However, relying solely on local texture information may negatively impact their subsequent classification because a texture is characterized by local information and its global appearance representing the repetition and the relationship between local patterns [20]. Another factor that can penalize the classification of textural images is noise, which distorts the observed data. Usually, noise is inherent to the process of acquiring real-life images. In most cases, conventional and current classification methods still present performance problems for classifying images with noisy textures. In addition to the aspects mentioned earlier, such descriptors often suffer from limitations such as computational complexity and limited robustness to changes in scale, rotation, and illumination.

In recent years, bio-inspired texture descriptors have emerged as a promising alternative, leveraging the inherent capabilities of the human visual system to better characterize and discriminate between different textures. However, despite the success of some bio-inspired methods, there is still room for improvement in terms of accuracy, robustness, and computational efficiency.

To circumvent most problems described above, Ataky and Lameiras Koerich [21] proposed a bio-inspired texture (BiT) descriptor, a generic descriptor that can describe both global and local texture information on various images [22,23]. Such a descriptor relies on biodiversity measures and taxonomic indices that can be interpreted and explained based on corresponding ecological concepts. The authors stated that textural patterns behave like ecological patterns. Therefore, large units can self-organize into assemblages that produce patterns from non-deterministic and nonlinear processes. From the ecosystem point of view, the proposed strategy performs well regardless of the challenges mentioned above on texture classification since biodiversity indices deal with such complexity. Furthermore, the BiT descriptor benefits from the invariance characteristics of ecological patterns to construct a rotation-, translation-, and permutation-invariant descriptor. In addition, it has shown benefits relative to several texture descriptors and deep approaches.

Diversity describes the multiplicity and abundance of species in a distinct unit of analysis. It is a measurement frequently employed to explain the complexity of a community [24]. Evenness counts the relative abundance of the different species in the same area and is a way to measure how the species are evenly distributed in a community. In other words, it shows the equitability of the taxa frequencies in a community [25]. Despite the concept of diversity being somewhat precise, Wagner et al. [25] presented a few reasons that may constrain its application: (i) the existence of multiple typically utilized diver-

sity indices that can produce different results; (ii) partitioning diversity into elements, such as evenness and richness, may be helpful, but changes depending on the diversity measure; and (iii) the terminology presently in use to characterize diversity is confusing and complex. For instance, with Shannon and Simpson, both indexes of diversity work differently. The former equally weights evenness and richness, whereas the latter gives more importance to evenness, and such differences in weighting clarify differences often perceived in results from each measure. What if we integrate and combine more diversity indices? In this paper, we state that incorporating more diversity and evenness indexes into the existing BiT descriptor, considering the variations in the mathematical properties of such indices, improves its global representation and leads to a more robust descriptor than the original one.

In light of the above, our study proposes a novel extended bio-inspired texture descriptor named E-BiT, which aims to address the limitations of existing approaches, including its baseline BiT, while maintaining high accuracy and robustness in texture analysis and characterization. Specifically, our goals are (i) to develop a descriptor that effectively captures a texture's local and global information while being robust against geometrical transformation, noise, and illumination changes; (ii) to ensure computational efficiency and make the proposed descriptor suitable for real-time applications; (iii) to rigorously evaluate the performance of the E-BiT descriptor on benchmark datasets and compare it with existing state-of-the-art methods.

The main contribution of this paper is an extension of the BiT descriptor [21] that integrates a few sets of diversity and evenness measures widely used in ecology to resemble the completeness of alpha diversity. Including such measures in the BiT descriptor [21] improves its global representativeness and produces a more robust texture characterization and classification. More precisely, the contributions are (i) an extended version of the BiT descriptor (henceforth E-BiT) combining species diversity, evenness, richness, and taxonomic indexes to resemble the completeness of alpha diversity as a generalization of biodiversity analysis; (ii) a descriptor that captures the all-inclusive compartment of texture image patterns (both local and global features); (iii) the E-BiT descriptor is invariant to permutation, scale, and translation; (iv) the E-BiT descriptor is straightforward to calculate and has low computational complexity; (v) the E-BiT descriptor is a generic texture descriptor that works well on diverse image types, from natural textures to medical images. We validated the proposed E-BiT descriptor on breast cancer histopathologic and natural image datasets. The E-BiT descriptor achieved state-of-the-art results surpassing the BiT descriptor [21], which confirms the relevance of including such diversity and evenness measures.

The organization of the rest of this paper is as follows. Section 2 presents the alpha and evenness diversity indices that are integrated into the BiT descriptor. Section 3.2 presents the experimental results of the E-BiT descriptor on three natural texture datasets and one HI dataset to assess its performance. The performance of the E-BiT descriptors is compared with other texture descriptors, such as the BiT descriptor, and CNN-based approaches. Finally, the conclusions are presented in the last section.

2. Proposed Texture Descriptor

The approach proposed in this work is inspired by our recent work [21], where we relied on the biodiversity measures and taxonomic indices to build a novel generic texture descriptor with several advantages over existing texture descriptors [21]. Some essential properties of such a descriptor are (i) the benefit of invariant characteristics of ecological patterns to construct a descriptor invariant to rotation, permutation, and translation; (ii) its ability to grab the all-inclusive behavior of texture image patterns regardless of the latter constituting a non-deterministic complex system. These properties allow the characterization of the intrinsic properties of the whole image.

The BiT descriptor [21] consists of fourteen ecological diversity indices comprising biodiversity measures and taxonomic indices. Nonetheless, other diversity indices commonly used in ecology may bring more information related to diversity characterization.

Would that additional information be relevant to texture characterization? What if we integrate and combine more diversity indexes? Therefore, we extend the BiT descriptor [21] by integrating more diversity and evenness indices. This paper explores new diversity and evenness indices not used in our previous work by considering the differences in their mathematical properties relative to the indices already used in the BiT descriptor. The combination of fourteen indices used to build the BiT descriptor [21] and ten novel indices give rise to the Extended BiT (E-BiT) descriptor, which provides an improved representation that leads to classification accuracy superior to the existing BiT descriptor.

2.1. Extended Bio-Inspired Texture (E-BiT) Descriptor

Biodiversity is characterized as the variety within and among life forms in an ecosystem or an area. It is calculated as a mixture of evenness and richness across species [26]. The former component is also referred to as species richness. It stands for the number of groups of functionally related individuals, and the latter denotes the proportions of species or functional groups present in an ecosystem or community. Besides these components, another type of index is taxonomic, which considers the taxonomic relationships between different organisms in an ecosystem. Moreover, taxonomic diversity denotes the average taxonomic distance between any two organisms randomly selected from a sample. Such a distance represents the length of the pathway joining these two organisms along the branches of a phylogenetic tree [27].

The multitude of indices proposed in biodiversity is one of the reasons why it is a bit difficult to quantify it. Ecological diversity indexes are mathematical estimates of species diversity and rely on abundance (number of individuals per species) and richness (number of species). The majority of indices employed in ecology usually estimate proportional abundances. Nonetheless, two main sorts of indices are dominance indices (e.g., the Simpson index) and information statistic indices (e.g., the Shannon–Weiner index).

Multiple diversity indices of richness can be measured. However, no obvious agreement exists about which indices are more appropriate and informative [28]. Notwithstanding, richness is the most straightforward metric commonly applied to represent diversity, whereas evenness describes the extent to which individuals are divided among species, that is, the individuals' distribution pattern. Lower values indicate that one or a few species dominate. Higher values suggest that relatively comparable numbers of individuals belong to each species and, consequently, a more practical measure of evenness in multiple contexts.

Therefore, the question that arises is “which one to choose to quantify the diversity?” Both richness and evenness represent two (among many) of biodiversity's aspects. Accordingly, no single number can integrate them both without information loss. However, taken jointly, they provide a robust suite of methods to explore and analyze the structure of a community. Likewise, Morris et al. [28] stated that standard diversity indices might appear switchable in simple analyses. Nevertheless, assuming complex interactions, the choice of the index can significantly modify the understanding of the outcomes. Thus, data mining should be avoided to determine the index yielding the most effective results. However, Morris et al. [28] indicated that analyzing multiple indices simultaneously provides a more significant understanding of the interactions in a system.

This work integrates ten more diversity and evenness indices to gain greater insight into a system's interactions (a textural image). Such diversity measures [24,29] are described as follows. We consider an image as an abstract model of an ecosystem [21], where pixels and gray levels correspond to individuals and species in an ecosystem, respectively. Furthermore, we use the same terminology and notation found in [21].

2.1.1. Alpha Diversity Indices

The Brillouin index (d_{HB}) is defined as

$$d_{HB} = \frac{\ln N! - \sum_{i=1}^S \ln n_i!}{N} \quad (1)$$

where N denotes the total number of pixels in the sample, S denotes the number of gray levels, and n_i represents the number of pixels in the i -th gray level.

The Strong's dominance index (d_{Dw}) is depicted as

$$d_{Dw} = \max_i \left[\left(\frac{b_i}{N} \right) - \frac{i}{S} \right] \quad (2)$$

where b_i denotes the sequential cumulative sum of the i -th different values of gray levels organized from the largest to the smallest. The term in brackets is calculated for all gray levels, and \max_i represents the maximum value in brackets for any gray level.

The Simpson's index (d_C) and the Enspie index (d_{ENS}) are defined as

$$d_C = 1 - \sum_{i=1}^S p_i^2 \quad (3)$$

$$d_{ENS} = \frac{1}{\sum_{i=1}^S p_i^2} \quad (4)$$

where p_i is the proportion of the community characterized by gray level i .

The McIntosh dominance diversity index (d_{McInt}) [30] is defined as

$$d_{McInt} = \frac{N - U}{N - \sqrt{N}} \quad (5)$$

where N denotes the total number of pixels in the image, $U = \sqrt{\sum n_i^2}$, and n_i is the number of pixels in the i -th species.

2.1.2. Evenness Indices

The Chao1 richness estimator (e_{CR}) [31,32] uses the observed richness (S_{obs}) and the number of singletons (F_1) and doubletons (F_2) to write the estimator for the class richness:

$$e_{CR} = S_{obs} + \frac{F_1^2}{2F_2} \quad (6)$$

where F_1 and F_2 are the count of singleton and doubleton gray levels in the image, respectively. According to Chao et al. [33], in the presence of many class abundance distributions, this estimator, initially derived as an estimation of minimum feasible richness (number of pixels pertaining to that specific gray level), is more intense if the reference sample size is large enough. This corroborates the reason for its use as a valid estimator for an extensive number of gray levels.

The Gini coefficient (e_{GC}) [34] is defined as

$$e_{GC} = \frac{2}{mS^2} \left(\sum_{i=1}^n (S+1-i)x_i \right) - \frac{1}{S} \quad (7)$$

where x_i is the number of pixels of the i -th gray level ranked from least to most abundant, $i \in [1, S]$, and m is the mean abundance of a gray level—the mean of the x_i values. The Gini coefficient measures income inequality and can also be used to measure any form of uneven

distribution. It ranges between 0 and 1, where 0 denotes a perfect inequality and 1 denotes a perfect equality, where each gray level has the same number of pixels.

The Heip’s evenness (e_{HE}) is defined as

$$e_{HE} = \frac{e^H - 1}{S - 1} \tag{8}$$

where H is the Shannon–Wiener entropy of counts using logarithm base e .

The Pielous evenness ($e_{P’}$) is defined as

$$e_{P’} = \frac{H}{\ln S} \tag{9}$$

Finally, the Simpsons evenness e_{SE} is defined as

$$e_{SE} = \frac{1}{S_{obs} D} \tag{10}$$

where D is dominance and S_{obs} is the number of observed gray levels.

All these indices are global measures computed on the whole image for a single channel for gray-level images and three channels for color images. Then, these ten scalar values are concatenated with the global and local BiT descriptors to build the 66-dimensional E-BiT descriptor.

3. Experimental Protocol

In this section, we show how the proposed E-BiT descriptor can be used in conjunction with other image processing and machine learning techniques to perform the texture classification task. The classification scheme is the same employed in [21] to evaluate the BiT and other texture descriptors, and it is structured into five stages: image channel splitting, preprocessing, feature extraction, normalization, and training/classification. Figure 1 shows an overview of the proposed scheme.

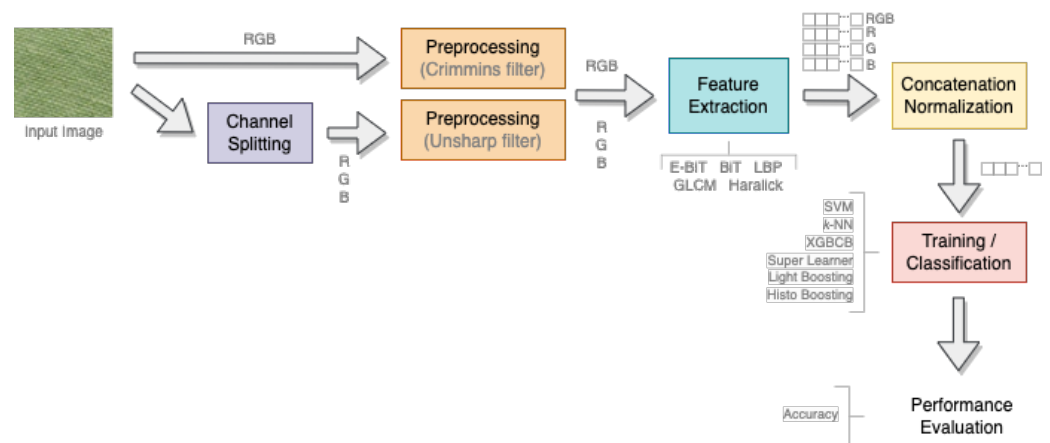


Figure 1. General architecture to evaluate the proposed E-BiT descriptor. The same architecture is employed in [21].

To evaluate the E-BiT descriptor, we used three benchmark texture datasets and a histopathological image dataset. The datasets were chosen due to their diverse and challenging textures, which allowed us to test the performance of the proposed descriptor rigorously.

We followed a standard experimental protocol defined in [21] for each dataset to ensure a fair comparison with other methods. We divided the dataset into training and test sets for each experiment, maintaining the same proportion of samples used in the literature.

For natural texture images, we randomly selected 70% of the samples for training for each texture class and used the remaining 30% for testing. Regarding the histopathological images, we use k -fold cross-validation with $k = 5$ and 10.

3.1. Performance Evaluation and Statistical Analysis

To assess the performance of the E-BiT descriptor, we calculated the classification accuracy, which is the ratio of correctly classified samples to the total number of samples in the test set. We used different classifiers, which have been widely used in texture analysis research and allow for a fair comparison with other methods.

To ensure the statistical validity of our results, we repeated each experiment ten times with different random train–test splits. We calculated the mean classification accuracy and standard deviation for each experiment. The results were compared with those of other state-of-the-art methods using the paired McNemar test at a significance level of 0.05. The paired McNemar test allowed us to determine if the differences in classification accuracy between the E-BiT descriptor and other methods were statistically significant.

3.2. Datasets

We used four datasets to assess the performance of the proposed E-BiT descriptor, including histopathological images (HIs) and natural texture images. These datasets have previously been utilized to evaluate other texture descriptors, including Haralick, GLCM, and LBP [12].

The Salzburg dataset (Figure 2a) is made up of 476 color texture images of 10 categories with a resolution of 128×128 pixels, where 70% are used for development (training and validation) and 30% for test. The Outex_TC_00010_c dataset (Figure 2b) contains a training set of 480 non-rotated color images belonging to 24 classes (20 per class). The test set includes 3840 color images in eight different orientations (5° , 10° , 15° , 30° , 45° , 60° , 75° , and 90°). The KTH-TIPS dataset (Figure 2c) contains 810 color images of 200×200 pixels, where 70% are used for training and 30% for testing. The images were captured in three different lighting directions at nine scales and in three different poses, with 81 images per class.

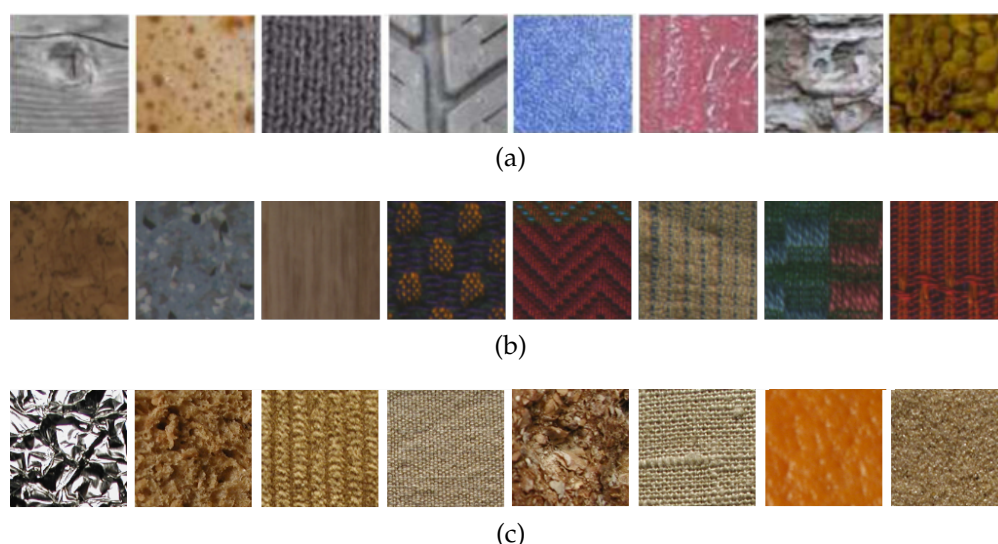


Figure 2. Samples of natural texture images from (a) Salzburg dataset, (b) Outex_TC_00010_c dataset, and (c) KTH-TIPS dataset.

The last dataset is the CRC [35] (Figure 3), which contains 5000 colorectal cancer histopathology images (HIs) cropped into patches of 150×150 pixels labeled into to 8 structure types: stroma (ST), complex stroma (C), tumor (T), lymphoid or immune cells (L), debris (D), adipose (AD), mucosa (M), and background or empty structures (E). HIs

usually have structures like nuclei (shape) and tissue variations (colors) within the same classes, making them more challenging than pure texture images [36].

Each structure described in the CRC dataset has a distinct textural feature. For instance, few shape characteristics can be found in the formation of cell nuclei, having a circular shape but distinct color due to hematoxylin. The CRC dataset has 625 images for each of the 8 structure types, summing up to 5000 images. The experiments with the CRC dataset were carried out using stratified 10-fold and 5-fold cross-validation (CV) to allow a fair comparison with state-of-the-art approaches. Figure 3 illustrates samples from the CRC dataset for each class.

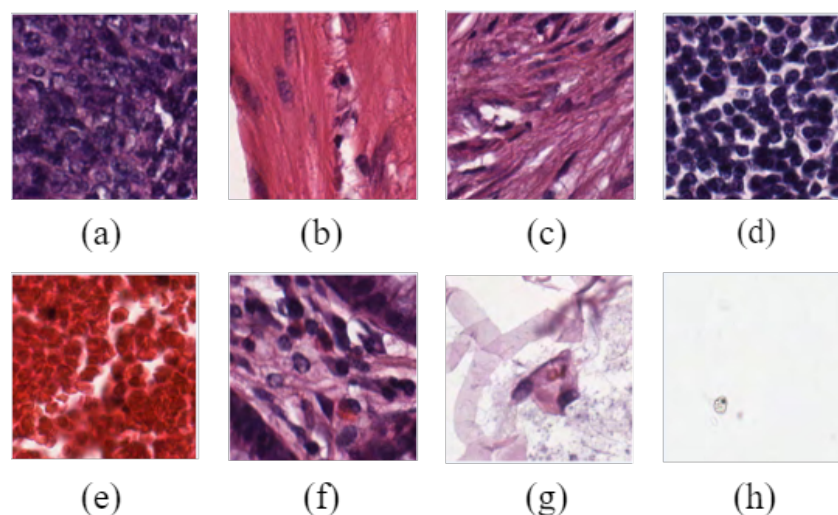


Figure 3. Sample HIs from the CRC dataset: (a) tumor, (b) stroma, (c) complex, (d) lympho, (e) debris, (f) mucosa, (g) adipose, (h) empty.

We compared the E-BiT descriptor's performance with the original BiT descriptor [21], which has already achieved state-of-the-art performance on the three texture datasets described above. Our main contribution lies in integrating ten more diversity and evenness indices to build a more discriminant texture descriptor capable of classifying textures efficiently due to its ability to capture the all-inclusive compartment of texture patterns, regardless of the latter constituting a non-deterministic complex system. Moreover, like the original BiT descriptor, the E-BiT descriptor is also permutation-, rotation-, and reflection-invariant. We followed the same scheme used for the BiT descriptor [21] for feature extraction.

4. Experimental Results

To demonstrate the benefits of the newly integrated indices, Table 1 compares the average accuracy achieved by the E-BiT descriptor and different classification algorithms with the accuracy achieved by BiT, GLCM, LBP, and Haralick descriptors with the same classification algorithms on the KTH-TIPS, Outex, and Salzburg datasets.

The proposed E-BiT descriptor achieved the best result on the Salzburg dataset with SuperL (95.79%). It outperformed the best BiT descriptor (94.23%), with a difference of 1.56%, and all other texture descriptors. The accuracy differences between E-BiT+SuperL and GLCM+k-NN and Haralick+SVM are nearly 20% and 8%, respectively. On the Outex dataset, the E-BiT descriptor also provided the best accuracy. The accuracy differences between the E-BiT and the other descriptors range from 0.12% to 16.79% for BiT+SVM and LBP+SuperL, respectively. Finally, the E-BiT descriptor surpassed all other descriptors on the KTH-TIPS dataset. For example, the E-BiT+SVM achieved the best accuracy of 98.92%, which is 1.05%, 4.03%, and 12.14% higher than the accuracy achieved by BiT+SVM, Haralick+SVM, and GLCM+SuperL, respectively.

The McNemar test, with a significance threshold of 95%, also revealed that the fraction of errors in each dataset is unique. As a result, the E-BiT descriptor shows a statistically

significant advantage over the other compared feature descriptors when it comes to the top performing results.

Figure 4 illustrates the average accuracy of all the descriptors presented in Table 1. In this figure, the E-BiT descriptor consistently outperforms the other methods in terms of average accuracy across all four datasets, indicating its effectiveness in a wide range of situations.

Table 1. Average accuracy (%) on the test set of KTH-TIPS, Outex, and Salzburg datasets. The best result for each texture descriptor is in boldface.

Dataset	Texture Descriptor	Classification Algorithm				
		HistoB	LightB	SuperL	<i>k</i> -NN	SVM
Salzburg	LBP	56.89	57.21	64.12	32.23	62.12
	GLCM	68.33	71.77	75.04	75.38	63.68
	Haralick	82.27	84.27	86.88	82.54	87.99
	BiT	88.20	90.17	94.23	88.65	92.33
	Proposed E-BiT	89.32	91.96	95.79	89.76	94.20
Outex	LBP	57.80	57.35	83.21	48.20	82.41
	GLCM	94.13	95.52	94.29	94.37	94.06
	Haralick	96.69	96.53	95.5	96.92	96.71
	BiT	99.68	98.53	99.53	99.83	99.88
	Proposed E-BiT	100.0	99.72	100.0	99.69	100.0
KTH-TIPS	LBP	59.51	57.18	64.83	58.26	61.78
	GLCM	83.12	86.00	86.83	74.89	79.83
	Haralick	88.83	90.94	93.00	89.71	94.89
	BiT	92.59	94.65	95.41	95.49	97.87
	Proposed E-BiT	94.77	94.50	96.45	96.51	98.92

k-NN with *k* = 1, 3, and 5 for KTH-TIPS, Salzburg, and Outex datasets, respectively. SVM with linear kernel and *c* = 1.3, 1.7, and 2.0 for Outex, KTH-TIPS, and Salzburg datasets, respectively.

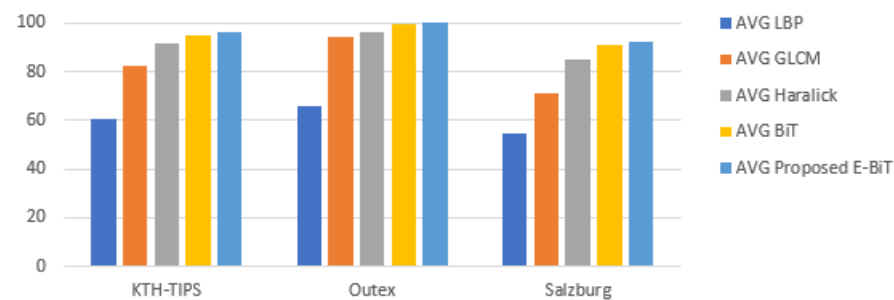


Figure 4. Average accuracy of HistoB, LightB, SuperL, *k*-NN, and SVM on KTH-TIPS, Outex, and Salzburg datasets. AVG before each descriptor stands for average accuracy.

Comparing the results presented in Table 1 with other approaches that have used identical datasets may not be appropriate due to disparities in the experimental protocols. For instance, most results reported on the Salzburg dataset overlook the subclasses used in the experimentations and the examples used in the test set. Mehta and Egiazarian [37] proposed a method based on a rotation-invariant LBP with a *k*-NN that achieved an accuracy of 96.26% on the Outex dataset. However, it has the disadvantage of not exploiting global features and color information. Du et al. [38] proposed an illumination-invariant, impulse noise-resistant, and rotation-invariant method based on a local spiking pattern with a neural network, which achieved an accuracy of 86.1% on the Outex dataset. Nonetheless, it does not consider color textures and has many hyperparameters. Hazgui et al. [39] defined a method based on genetic programming and combining LBP and HOG features. With a *k*-NN, such an approach achieved 91.20% accuracy on the KTH-TIPS dataset. Nonetheless, color information and global features are not taken into account. Nguyen et al. [40] proposed rotation- and noise-invariant statistical binary patterns. This method achieved an

accuracy of 97.73% on the KTH-TIPS dataset, which is approximately 1.19% lower than that achieved by the E-BiT+SVM. However, this method has high computational complexity and is resolution-sensitive. Qi et al. [41] used Shannon entropy and LBP to encode cross-channel texture correlation and investigated the relative variance of texture patterns among color channels. They proposed a multi-scale rotation-invariant cross-channel LBP (CCLBP). They compute the LBP descriptors for each channel, three scales, and consider co-occurrence statistics. Such an approach achieved 99.01% accuracy on the KTH-TIPS dataset with an SVM, which is nearly equal to the accuracy achieved by the E-BiT+SVM. Nonetheless, this approach is not scale-invariant.

Table 2 presents and compares the performance of BiT and E-BiT descriptors. Although the accuracy differs in 3.69% and 3.13% for k -NN and SVM classifiers, respectively, and 3.04%, 1.90%, 1.07%, and 0.20% for LightB, XGBCB, SuperL, and HistoB ensemble classifiers, respectively, the E-BiT descriptor wins in all the cases. Another remark is that, unlike the BiT descriptor, the E-BiT descriptor obtained its best accuracy with a monolithic classifier (SVM), even though E-BiT+SuperL also outperformed BiT+SuperL, which provided the best average accuracy for the BiT descriptor. Furthermore, the McNemar test for the CRC dataset under SVM shows that, with the exception of the SuperL, all classifiers produce a similar percentage of errors on the test set. Thus, there is no statistically significant gap between the E-BiT descriptor's best results and any other classifier on the CRC dataset. The discrepancies between SVM and SuperL, however, are statistically significant.

Table 2. Average accuracy (%) of ensemble methods and monolithic classifiers with the BiT and E-BiT descriptors on the CRC dataset. Best results for BiT and E-BiT descriptors are shown in boldface.

Texture Descriptor	Classification Algorithm					
	XGBCB	HistoB	LightB	SuperL	k -NN	SVM
BiT	90.50	90.71	90.23	92.52	83.70	90.98
Proposed E-BiT	91.59	90.91	93.27	93.59	87.39	94.11

Table 3 compares the best result of Table 2 achieved with the E-BiT+SVM to the state-of-the-art for the CRC dataset. The E-BiT outperforms almost all other methods in terms of accuracy. For example, considering an eight-class classification task and a ten-fold CV, the difference in accuracy to the second-best method (shallow) is 1.15%, and the difference is 1.71% to the third-best method (CNN). In addition, the E-BiT descriptor slightly outperformed the second-best method (CNN) for 5-fold CV, with a difference of 0.67%. The results highlight the advantages of the E-BiT descriptor over other shallow and deep methods.

Table 3. Average accuracy (%) of state-of-the-art deep and shallow approaches on the CRC dataset (8-class).

Reference	Approach	10-Fold CV	5-Fold CV
Pham [42]	CNN	–	84.00
Raczkowski [43]	CNN	92.40	92.20
Wang et al. [44]	CNN	–	92.60
Sarkar and Acton [45]	Shallow	73.60	–
Kather et al. [35]	Shallow	87.40	–
Ataky and Lameiras Koerich [21]	Shallow	92.96	–
Proposed E-BiT+SVM	Shallow	94.11	93.27
Kather et al. [35]	Shallow	96.90 *	–
Ribeiro et al. [46]	Shallow	97.60 *	–

* Results for 2-class classification (malignant and benign).

Finally, we conducted an empirical evaluation to estimate the computational time required by the E-BiT descriptor for feature extraction and compare it to the computational time required by its baseline for the three texture datasets. The following is the average time per image for executing a Python implementation of Algorithm 1, including preprocessing: (i) KTH-TIPS dataset: 1.39 s and 1.42 s for BiT and E-BiT, respectively; (ii) Outex dataset: 461.8 ms and 498.8 ms for BiT and E-BiT, respectively; and (iii) Salzburg dataset: 881 ms and 910 ms for BiT and E-BiT, respectively. The methodology was developed using the Microsoft Windows 10 operating system and the Python programming language running on an Intel Core i7-8850H CPU @ 2.60 GHz, 64-bit operating system, x64-based processor, and 32 GB of RAM.

4.1. Analysis of the Experimental Results

The experimental results on diverse datasets showed that the E-BiT descriptor is generalizable and applicable to various texture analysis tasks. The reasons behind the improved performance and the potential advantages of using the proposed E-BiT descriptor for texture analysis and characterization are as follows. (i) The E-BiT's design enables extracting more discriminative features by incorporating local and global texture information. It is achieved by combining the properties found in descriptors such as LBP, GLCM, and Gabor filters, resulting in a more comprehensive texture representation and better texture characterization and analysis. Compared to the baseline BiT, the E-BiT integrates ten more diversity and evenness indices to gain greater insight into gray-level interactions within a textural image. (ii) The evaluation demonstrated that the proposed E-BiT descriptor is robust and adaptable across various datasets, image conditions, and application scenarios. As shown in Tables 1–3, the E-BiT descriptor consistently outperforms the other methods regarding average accuracy across all four datasets, indicating its effectiveness in various situations. (iii) When comparing the E-BiT descriptor with other methods, it combines the strengths of these methods and addresses their limitations, resulting in better overall performance. (iv) The E-BiT's performance was thoroughly evaluated using diverse datasets, demonstrating its generalizability and applicability to a wide range of texture analysis tasks. The consistently high accuracy across different datasets highlights the descriptor's robustness and ability to capture essential features of various texture types.

The advantages of the shallow approaches that use the E-BiT descriptor over CNNs are also noteworthy. CNNs have remarkable performance on object detection and recognition tasks. However, the shape information extracted by CNNs is of minor importance in texture analysis [15]. For instance, Andrearczyk and Whelan [15] developed a simple texture CNN (T-CNN) architecture for analyzing texture images that pools an energy measure at the last convolution layer and discards the overall shape information analyzed by classic CNNs. Despite the promising results, the trade-off between accuracy and complexity is unfavorable. Other T-CNN architectures have also achieved moderate performance in texture classification [16,17,19,47]. For instance, de Matos et al. [16] and Ataky et al. [47] carried out experiments on the three texture datasets with a tiny T-CNN of 11,900 parameters, trained without and with data augmentation (1×, 2×, 4×, and 6×). Such a tiny T-CNN achieved the best accuracy of 61.06%, 70.60%, and 70.22% for Salzburg, Outex, and KTH-TIPS datasets, respectively. These results are far below the accuracy achieved by E-BiT+SVM and E-BiT+SuperL, as reported in Table 1.

CNNs have shown promising results in texture recognition tasks, but their performance depends on the dataset's complexity and the specific characteristics of the textures. In some cases, shallow approaches that employ traditionally handcrafted texture descriptors, like LBP, Gabor filters, or GLCM, still provide competitive results, especially when datasets are small, or the textures are less complex. It is worth noting that massive labeled datasets are not always possible in medical imaging. Some challenges and limitations need to be addressed when using CNNs on texture classification tasks. (i) They have a large number of parameters to be learned on limited training data, which makes the model memorize the training data instead of generalizing well on unseen data. However, data

augmentation, dropout, and regularization can mitigate overfitting. (ii) They typically require a large amount of labeled data to learn the complex patterns and features within the data. With small datasets, the performance may be less optimal. However, transfer learning, where pre-trained models are fine-tuned on the target dataset, can help improve performance in such cases. (iii) They are computationally expensive to train and may require specialized hardware, such as GPUs, for efficient training. Traditionally handcrafted descriptors might be more computationally efficient for small datasets or less complex texture analysis tasks. (iv) They still lack explainability and interpretability, especially in the medical field.

4.2. Invariance Properties of the E-BiT Descriptor

We have also evaluated the invariant properties of new aggregated alpha and evenness diversity indices. We applied different geometric transformations to each image, namely rotation of 90° and 180° , horizontal and vertical reflection, rescaling by 50%, and computing the values of all newly integrated features. The non-normalized values of the descriptors are shown in Tables 4 and 5 for images taken randomly from KTH and CRC datasets, respectively.

Table 4. Non-normalized values of the E-BiT descriptors computed for a texture image (original) and six transformed texture images.

E-BiT Descriptors	Original	Transformations				
		Rotation		Reflection		Rescaling 50%
		90°	180°	Horizontal	Vertical	
d_{HB}	9.6646	9.6646	9.6646	9.6646	9.6646	8.2780
e_{Dw}	0.0364	0.0364	0.0364	0.0364	0.0364	0.0372
d_C	0.9999	0.9999	0.9999	0.9999	0.9999	0.9998
d_{ENS}	16263.1	16263.1	16263.1	16263.1	16263.1	4064.3
e_{CR}	16384.0	16384.0	16384.0	16384.0	16384.0	4096.0
e_{GC}	0.0493	0.0493	0.0493	0.0493	0.0493	0.0503
d_{McInt}	0.9999	0.9999	0.9999	0.9999	0.9999	0.9997
e_{HE}	0.9963	0.9963	0.9963	0.9963	0.9963	0.9962
e_J	0.9996	0.9996	0.9996	0.9996	0.9996	0.9995
e_{SE}	0.9926	0.9926	0.9926	0.9926	0.9926	0.9923

Table 5. Non-normalized values of the E-BiT descriptors computed for an HI (original) and six transformed HIs.

E-BiT Descriptors	Original	Transformations				
		Rotation		Reflection		Rescaling 50%
		90°	180°	Horizontal	Vertical	
d_{HB}	10.3017	10.3017	10.3017	10.3017	10.3017	8.9275
e_{Dw}	0.0509	0.0509	0.0509	0.0509	0.0509	0.0477
d_C	1.0000	1.0000	1.0000	1.0000	1.0000	0.9999
d_{ENS}	30136.5	30136.5	30136.5	30136.5	30136.5	7631.3
e_{CR}	30625.0	30625.0	30625.0	30625.0	30625.0	7744.0
e_{GC}	0.0703	0.0703	0.0703	0.0703	0.0703	0.0663
d_{McInt}	1.0001	1.0001	1.0001	1.0001	1.0001	1.0001
e_{HE}	0.9921	0.9921	0.9921	0.9921	0.9921	0.9928
e_J	0.9992	0.9992	0.9992	0.9992	0.9992	0.9992
e_{SE}	0.9840	0.9840	0.9840	0.9840	0.9840	0.9850

The values of the E-BiT descriptor illustrated in Tables 4 and 5 show that all measurements are reflection- and rotation-invariant, as they have similar values for original texture images and HIs. This also substantiates the fact that the E-BiT descriptors capture the all-inclusive comportment of patterns within an image. Simpson index (d_c), Gini coefficient

(e_{GC}), Heip's evenness (e_{HG}), Pielous evenness (e_j), McIntosh dominance diversity (d_{McInt}), and Simpson evenness (e_{SE}) are scale-invariant, as they provided values in the order of the original images. On the other hand, most diversity measures based on abundance and richness exhibit some scale dependence. By rescaling the original image, we affect the proportion of both factors, which affects the resulting values either inversely or directly. However, normalizing such measurements by the total number of pixels can mitigate this effect. On the other hand, indexes based on evenness are based on the equitability of taxa frequencies in a community. As a result, they are unaffected by the change in scaling because evenness is determined by the intrinsic properties of the ecosystem (image).

5. Discussion

The E-BiT's outstanding performance can be attributed to its ability to capture the all-inclusive behavior of texture image patterns at local and global levels. This ability is achieved by combining ecological concepts of species diversity, evenness, richness, and taxonomic indexes. These concepts offer a more holistic understanding of texture patterns and their relationships within an image, allowing the E-BiT descriptor to classify textures more effectively. Furthermore, the E-BiT invariance to scale, translation, and permutation contributes to its robustness and adaptability in various applications, such as natural and HI analysis. This is an advantage over other methods, which may need to account for these invariances.

However, the E-BiT descriptor also has its limitations. First, it relies on preprocessing techniques for normalization and geometric transformations, which may introduce additional complexity to the overall texture characterization process. This could be a disadvantage compared to other methods that do not require extensive preprocessing. In addition to such limitations, the E-BiT descriptor presents further disadvantages that should be considered. (i) It is unable to define dynamic ranges of the biodiversity and taxonomic indices. The ranges depend on the texture variability, which may limit the descriptor's applicability in some cases. This issue necessitates further normalization. Thus, in future work, we will search to develop adaptive strategies for defining the indices' ranges based on the image characteristics. (ii) It does not inherently provide a tolerance parameter to cope with noise in some types of images. That means preprocessing techniques may be required to address noise-related issues, adding complexity to the overall texture characterization process. (iii) The invariance to changes in image contrast is not yet conclusive, as its performance depends on the specific datasets being analyzed. This limitation highlights the need for further investigation into how the descriptor responds to different image contrasts and potential strategies for enhancing its contrast invariance.

Taking these additional disadvantages into account, the E-BiT descriptor, while promising, requires continued research to address its limitations and further refine its performance across various applications and settings.

In summary, the E-BiT descriptor offers a promising contribution to texture characterization by leveraging ecological concepts for a more comprehensive understanding of texture patterns. However, while it demonstrates superior performance compared to existing methods, further research is needed to explore its limitations and potential improvements in various applications and settings.

6. Conclusions and Future Work

This paper proposed an extended version of the bio-inspired texture descriptor (E-BiT) to characterize textures in images. This extension, named E-BiT, combines global ecological concepts of species diversity, evenness, richness, and taxonomic indexes to approximate the completeness of diversity as a generalization of biodiversity analysis. That allows the development of a descriptor that captures the all-inclusive behavior of texture image patterns at local and global levels. Furthermore, the E-BiT descriptor is insensitive to scale, translation, or permutation.

Compared to related methods for texture characterization and its baseline version, the E-BiT descriptor emerges as a promising texture characterization tool, achieving state-of-the-art texture classification performance. In addition, its generic nature is notable, as it performs well in natural and histopathologic images.

Moreover, notwithstanding the meaningful results, there are still some aspects where the E-BiT descriptor could be improved and extended. For future work, we consider the following research directions as very promising:

(i) Examining how the E-BiT descriptor behaves at different spatial scales and resolutions, which may allow for the most effective texture property extraction while maintaining or improving performance;

(ii) Incorporating dynamic range selection for biodiversity and taxonomic indices to enhance the descriptor's adaptability to different texture variability within images;

(iii) Defining a tolerance parameter for the E-BiT descriptor to improve its robustness against noise without the need for preprocessing in certain types of images;

(iv) Studying the E-BiT descriptor's invariance to changes in image contrast across different datasets to establish a more conclusive understanding of its performance. We expect that our work on the E-BiT descriptor will inspire further research and contribute to the ongoing development of texture analysis and characterization methods.

Author Contributions: Conceptualization, S.T.M.A. and A.L.K.; Methodology, S.T.M.A.; Writing—original draft preparation, S.T.M.A. and A.L.K.; Writing—review and editing, S.T.M.A. and A.L.K.; Supervision, A.L.K.; All authors have read and agreed to the published version of the manuscript.

Funding: This research was partially funded by the Regroupement Strategique REPARTI—Fonds de Recherche du Québec—Nature et Technologie (FRQNT) and by the Natural Sciences and Engineering Research Council of Canada (NSERC), Discovery grant number RGPIN-2016-04855.

Data Availability Statement: The KTH-TIPS dataset is available at <https://www.csc.kth.se/cvap/databases/kth-tips/index.html>. Accessed on 2 May 2023. The Outex dataset is available at <https://color.univ-lille.fr/datasets/extended-outex> accessed on 2 May 2023. The Salzburg dataset is available at <https://www.wavelab.at/sources/STex/> accessed on 2 May 2023. The CRC dataset is available at https://zenodo.org/record/53169#.Y3MHVy_71qs accessed on 2 May 2023. The source codes are available at <https://github.com/stevetmat/BioInspiredFDesc> accessed on 2 May 2023.

Conflicts of Interest: The authors declare no conflicts of interest.

References

1. Traina, A.J.M. Suporte à Visualização de Consultas por Similaridade em Imagens Médicas Através de Estrutura de Indexação Métrica. Ph.D. Thesis, ICMC/USP, São Carlos, Brazil, 2001.
2. Tuceryan, M.; Jain, A.K. Texture analysis. In *Handbook of Pattern Recognition and Computer Vision*; World Scientific: Singapore, 1993; pp. 235–276.
3. Haralick, R.M.; Shanmugam, K.; Dinstein, I.H. Textural features for image classification. *IEEE Trans. Syst. Man Cybern.* **1973**, *6*, 610–621. [[CrossRef](#)]
4. Haralick, R.M. Statistical and structural approaches to texture. *Proc. IEEE* **1979**, *67*, 786–804. [[CrossRef](#)]
5. Pietikäinen, M.; Hadid, A.; Zhao, G.; Ahonen, T. *Computer Vision Using Local Binary Patterns*; Springer Science & Business Media: Berlin/Heidelberg, Germany, 2011; Volumr 40.
6. Arivazhagan, S.; Ganesan, L. Texture classification using wavelet transform. *Pattern Recognit. Lett.* **2003**, *24*, 1513–1521. [[CrossRef](#)]
7. Cross, G.R.; Jain, A.K. Markov random field texture models. *IEEE Trans. Pattern Anal. Mach. Intell.* **1983**, *1*, 25–39. [[CrossRef](#)] [[PubMed](#)]
8. Kaplan, L.M. Extended fractal analysis for texture classification and segmentation. *IEEE Trans. Image Process.* **1999**, *8*, 1572–1585. [[CrossRef](#)] [[PubMed](#)]
9. Tuncer, T.; Dogan, S.; Ataman, V. A novel and accurate chess pattern for automated texture classification. *Phys. A Stat. Mech. Its Appl.* **2019**, *536*, 122584. [[CrossRef](#)]
10. Tuncer, T.; Dogan, S.; Ertam, F. A novel neural network based image descriptor for texture classification. *Phys. A Stat. Mech. Its Appl.* **2019**, *526*, 120955. [[CrossRef](#)]
11. Tuncer, T.; Dogan, S. Pyramid and multi kernel based local binary pattern for texture recognition. *J. Ambient Intell. Humaniz. Comput.* **2020**, *11*, 1241–1252. [[CrossRef](#)]
12. Simon, P.; Uma, V. Review of texture descriptors for texture classification. In *Data Engineering and Intelligent Computing*; Springer: Berlin/Heidelberg, Germany, 2018; pp. 159–176.

13. Liu, L.; Chen, J.; Fieguth, P.; Zhao, G.; Chellappa, R.; Pietikäinen, M. From BoW to CNN: Two decades of texture representation for texture classification. *Int. J. Comput. Vis.* **2019**, *127*, 74–109. [[CrossRef](#)]
14. Olah, C.; Mordvintsev, A.; Schubert, L. Feature Visualization. *Distill* **2017**, *2*, e7. [[CrossRef](#)]
15. Andrearczyk, V.; Whelan, P.F. Using filter banks in Convolutional Neural Networks for texture classification. *Pattern Recognit. Lett.* **2016**, *84*, 63–69. [[CrossRef](#)]
16. de Matos, J.; de Souza Britto, A., Jr.; de Oliveira, L.E.S.; Koerich, A.L. Texture CNN for Histopathological Image Classification. In Proceedings of the 32nd IEEE Intl Symp on Computer-Based Medical Systems (CBMS), Cordoba, Spain, 5–7 June 2019; pp. 580–583. [[CrossRef](#)]
17. Fujieda, S.; Takayama, K.; Hachisuka, T. Wavelet convolutional neural networks for texture classification. *arXiv* **2017**, arXiv:1707.07394.
18. Vriesman, D.; Britto Junior, A.S.; Zimmer, A.; Koerich, A.L. Texture CNN for Thermoelectric Metal Pipe Image Classification. In Proceedings of the IEEE 31st Int'l Conf on Tools with Artificial Intelligence, Portland, OR, USA, 4–6 November 2019; pp. 569–574. [[CrossRef](#)]
19. de Matos, J.; Soares de Oliveira, L.E.; de Souza Britto Junior, A.; Lameiras Koerich, A. Large-Margin Representation Learning for Texture Classification. *Pattern Recognit. Lett.* **2023**, 1–8. *in press*. [[CrossRef](#)]
20. Liu, L.; Fieguth, P. Texture classification from random features. *IEEE Trans. Pattern Anal. Mach. Intell.* **2012**, *34*, 574–586. [[CrossRef](#)]
21. Ataky, S.T.M.; Lameiras Koerich, A. A novel bio-inspired texture descriptor based on biodiversity and taxonomic measures. *Pattern Recognit.* **2022**, *123*, 108382. [[CrossRef](#)]
22. Ataky, S.T.M.; Lameiras Koerich, A. Multiresolution texture analysis of histopathologic images using ecological diversity measures. *Expert Syst. Appl.* **2023**, *224*, 119972. [[CrossRef](#)]
23. Ataky, S.T.M.; Saqui, D.; de Matos, J.; Britto, A.d.S., Jr.; Koerich, A.L. Multiscale Analysis for Improving Texture Classification. *Appl. Sci.* **2023**, *13*, 1291. [[CrossRef](#)]
24. Magurran, A.E. *Measuring Biological Diversity*; John Wiley & Sons: Hoboken, NJ, USA, 2003.
25. Wagner, B.D.; Grunwald, G.K.; Zerbe, G.O.; Mikulich-Gilbertson, S.K.; Robertson, C.E.; Zemanick, E.T.; Harris, J.K. On the Use of Diversity Measures in Longitudinal Sequencing Studies of Microbial Communities. *Front. Microbiol.* **2018**, *9*. [[CrossRef](#)]
26. Rousseau, R.; Van Hecke, P.; Nijssen, D.; Bogaert, J. The relationship between diversity profiles, evenness and species richness based on partial ordering. *Environ. Ecol. Stat.* **1999**, *6*, 211–223. [[CrossRef](#)]
27. Sohier, C. Measurements of Biodiversity. 2019. Available online: http://www.coastalwiki.org/wiki/Measurements_of_biodiversity (accessed on 2 May 2023).
28. Morris, E.K.; Caruso, T.; Buscot, F.; Fischer, M.; Hancock, C.; Maier, T.S.; Meiners, T.; Müller, C.; Obermaier, E.; Prati, D.; et al. Choosing and using diversity indices: Insights for ecological applications from the German Biodiversity Exploratories. *Ecol. Evol.* **2014**, *4*, 3514–3524. [[CrossRef](#)]
29. SDR-IV. Species Diversity and Richness 4. 2020. Available online: <http://www.pisces-conservation.com/sdrhelp/index.html?bergerparker.htm> (accessed on 2 May 2023).
30. McIntosh, R.P. An index of diversity and the relation of certain concepts to diversity. *Ecology* **1967**, *48*, 392–404. [[CrossRef](#)]
31. Chao, A. Nonparametric estimation of the number of classes in a population. *Scand. J. Stat.* **1984**, *11*, 265–270.
32. Eren, M.I.; Chao, A.; Hwang, W.H.; Colwell, R.K. Estimating the richness of a population when the maximum number of classes is fixed: A nonparametric solution to an archaeological problem. *PLoS ONE* **2012**, *7*, e34179. [[CrossRef](#)]
33. Chao, A.; Shen, T.J.; Hwang, W.H. Application of Laplace's boundary-mode approximations to estimate species and shared species richness. *Aust. N. Z. J. Stat.* **2006**, *48*, 117–128. [[CrossRef](#)]
34. Gini, C. Variabilità e mutabilità. In *Reprinted in Memorie di Metodologica Statistica*; Pizetti, E., Salvemini, T., Eds.; Libreria Eredi Virgilio Veschi: Rome, Italy, 1955.
35. Kather, J.N.; Weis, C.A.; Bianconi, F.; Melchers, S.M.; Schad, L.R.; Gaiser, T.; Marx, A.; Zöllner, F.G. Multi-class texture analysis in colorectal cancer histology. *Sci. Rep.* **2016**, *6*, 27988. [[CrossRef](#)] [[PubMed](#)]
36. de Matos, J.; Ataky, S.T.M.; de Souza Britto, A.; Soares de Oliveira, L.E.; Lameiras Koerich, A. Machine Learning Methods for Histopathological Image Analysis: A Review. *Electronics* **2021**, *10*, 562. [[CrossRef](#)]
37. Mehta, R.; Egiazarian, K. Dominant rotated local binary patterns (DRLBP) for texture classification. *Pattern Recognit. Lett.* **2016**, *71*, 16–22. [[CrossRef](#)]
38. Du, S.; Yan, Y.; Ma, Y. Local spiking pattern and its application to rotation-and illumination-invariant texture classification. *Optik* **2016**, *127*, 6583–6589. [[CrossRef](#)]
39. Hazgui, M.; Ghazouani, H.; Barhoumi, W. Genetic programming-based fusion of HOG and LBP features for fully automated texture classification. *Vis. Comput.* **2021**, *37*, 1–20. [[CrossRef](#)]
40. Nguyen, T.P.; Vu, N.S.; Manzanera, A. Statistical binary patterns for rotational invariant texture classification. *Neurocomputing* **2016**, *173*, 1565–1577. [[CrossRef](#)]
41. Qi, X.; Qiao, Y.; Li, C.; Guo, J. Exploring Cross-Channel Texture Correlation for Color Texture Classification. In Proceedings of the British Machine Vision Conf, Bristol, UK, 9–13 September 2013; pp. 1–11. [[CrossRef](#)]
42. Pham, T.D. Scaling of texture in training autoencoders for classification of histological images of colorectal cancer. In Proceedings of the International Symposium on Neural Networks, Hokkaido, Japan, 21–26 June 2017; pp. 524–532.

43. Raczkowski, Ł.; Możejko, M.; Zambonelli, J.; Szczurek, E. ARA: Accurate, reliable and active histopathological image classification framework with Bayesian deep learning. *Sci. Rep.* **2019**, *9*, 1–12.
44. Wang, C.; Shi, J.; Zhang, Q.; Ying, S. Histopathological image classification with bilinear convolutional neural networks. In Proceedings of the 2017 39th Annual International Conference of the IEEE Engineering in Medicine and Biology Society (EMBC), Jeju Island, Republic of Korea, 11–15 July 2017; pp. 4050–4053.
45. Sarkar, R.; Acton, S.T. Sdl: Saliency-based dictionary learning framework for image similarity. *IEEE Trans. Image Process.* **2017**, *27*, 749–763. [[CrossRef](#)] [[PubMed](#)]
46. Ribeiro, M.G.; Neves, L.A.; do Nascimento, M.Z.; Roberto, G.F.; Martins, A.S.; Tosta, T.A.A. Classification of colorectal cancer based on the association of multidimensional and multiresolution features. *Expert Syst. Appl.* **2019**, *120*, 262–278. [[CrossRef](#)]
47. Ataky, S.T.M.; de Matos, J.; de Souza Britto Junior, A.; Soares de Oliveira, L.E.; Koerich, A.L. Data Augmentation for Histopathological Images Based on Gaussian-Laplacian Pyramid Blending. In Proceedings of the 2020 International Joint Conference on Neural Networks (IJCNN), Glasgow, UK, 19–24 July 2020; pp. 1–8. [[CrossRef](#)]

Disclaimer/Publisher’s Note: The statements, opinions and data contained in all publications are solely those of the individual author(s) and contributor(s) and not of MDPI and/or the editor(s). MDPI and/or the editor(s) disclaim responsibility for any injury to people or property resulting from any ideas, methods, instructions or products referred to in the content.